A Multifunctional Coordination Polymer Exhibiting Reversible Mechanical Motion Allowing Selective Uptake of Guests Leading to Enhanced Electrical Conductivity

Robert W. Elliott, [a] Ashley L. Sutton, [a] Brendan F. Abrahams,[a]* Deanna M. D'Alessandro,[b] Lars Goerigk, [a] Carol Hua, [a,b] Timothy A. Hudson, [a] Richard Robson,[a]* and Keith F. White[a,c]

[a] School of Chemistry, University of Melbourne, Parkville, Victoria 3010, Australia.
Email: bfa@unimelb.edu.au; r.robson@unimelb.edu.au; Tel: +61 3 8344 0341
[b] School of Chemistry, University of Sydney, Sydney, New South Wales 2006, Australia
[c] School of Molecular Science, La Trobe University, Wodonga, Victoria 3690, Australia
RWE and ALS are equal first authors.

Abstract

A remarkably flexible, multi-functional, 2D coordination polymer exhibiting an unprecedented mode of reversible mechanical motion, enabling pores to open and close, is reported. Such multi-functional materials are highly sought after, owing to the potential to exploit coexisting electronic and mechanical functionality that underpin useful technological applications such as actuators and ultra-sensitive detectors. The coordination polymer, of composition $Mn(F_4TCNQ)(py)_2$ (F_4TCNQ = 2,3,5,6-tetrafluoro-7,7,8,8-tetracycanoquinodimethane; py = pyridine), consists of Mn(II) centers bridged by F_4TCNQ dianions and coordinated by pyridine molecules that extend above and below the 2D network. Exposure of $Mn(F_4TCNQ)(py)_2$, in its collapsed state, to carbon dioxide results in a pore opening process at a threshold pressure for a given temperature. In addition to carbon dioxide, a variety of volatile guests may be incorporated into the pores, which are lined with electron-rich F_4TCNQ dianions. The inclusion of electron deficient guests such as 1,4-benzoquinone, nitrobenzene, maleic anhydride and iodine into the pores is accompanied by a striking color change associated with a new host-guest charge transfer interaction and an improvement in semi-conductor behavior, with the iodine adduct showing an increase in conductivity of almost five orders of magnitude. Experimental and density functional theory calculations on this remarkable multi-functional material demonstrate a reduction in the optical band gap with increasing electron affinity of the guest.

Introduction

In recent years there has been considerable interest in coordination polymers and metal organic frameworks (MOFs) that behave as multifunctional materials.[1] Through judicious choice of ligands and metal centers it is possible to produce materials that possess combinations of various chemical and physical properties such as selective adsorption[2, 3], electrical conductivity[4, 5], electroactivity[6], catalytic behavior[7-9] and magnetic ordering[10, 11]. One of the major attractions of metal-ligand network materials is that such systems commonly display network flexibility associated with the ability of metal ions and ligand components to move in response to guest uptake or loss without breaking coordinate and covalent bonds.[12, 13] When the flexible components also exhibit electroactivity then it is possible to generate a multifunctional material that not only changes its geometry upon exposure to certain guests but also its electrical and spectroscopic behavior. In such circumstances there is the prospect of establishing a relationship between the spectroscopic and electrical conductivity properties and the chemical nature of the guests.

A particularly attractive building block for functional coordination networks is 7,7,8,8-tetracyanoquinodimethane (TCNQ, **I** X = H, Scheme 1) which commonly yields charge-transfer solids that exhibit electrical conduction.[14, 15] In combination with tetrathiafulvalene (TTF), TCNQ forms a remarkable 1:1 solid that exhibits metal-like conductivity.[16] Its capacity to form electrically conducting charge transfer complexes is attributed to the accessibility of mixed valence states between its neutral quinoidal form (**I**) and its monoanionic radical form (**II**). In the charge transfer complex TTF-TCNQ a charge of -0.59 has been assigned to the TCNQ. Whilst attempts have been made to incorporate TCNQ or $TCNQ^{\cdot-}$ into coordination polymers, only a limited number of materials have been characterised.[17-25] The dianionic form of TCNQ is also known, however early reports described it as being very sensitive to oxidation.[26] More recent work has indicated that this aromatic dianion as well its tetrafluorinated analogue, 7,7,8,8-tetracyano-2,3,5,6-tetrafluoroquinodimethane (F_4TCNQ^{II-}, **III** X = F) may be stabilised through charge transfer interactions with electron acceptors or through coordination to metal centers within coordination networks where it may be generated by deprotonation of its acid form, X_4TCNQH_2 (**IV,** X = H or F). The deprotonation of **IV** in the presence of metal ions is an approach used to create more than 100 network materials involving the X_4TCNQ^{II-}.[27-34] Crystals of coordination polymers incorporating these dianions are typically pale unless they have the opportunity to participate in charge transfer interactions

with electron deficient species, in which case, the crystals can be intensely colored. It is important to emphasise that whereas the neutral forms of X_4TCNQ are electron deficient, allowing it to serve as an acceptor in charge transfer interactions, the X_4TCNQ^{II-} form is electron rich and therefore can act as a donor. In addition to the ability of the electroactive X_4TCNQ^{II-} ligand to participate in charge transfer interactions, previous structural investigations indicate that the ligands can coordinate to metal centers with significant distortions from linear coordination at the nitrogen donor atoms.[20] The variability in coordination angle at the nitrogen offers the prospect of structural flexibility and thus metal-X_4TCNQ^{II-} network materials have the potential to behave as dynamic network systems which can participate in charge-transfer interactions with guest molecules.

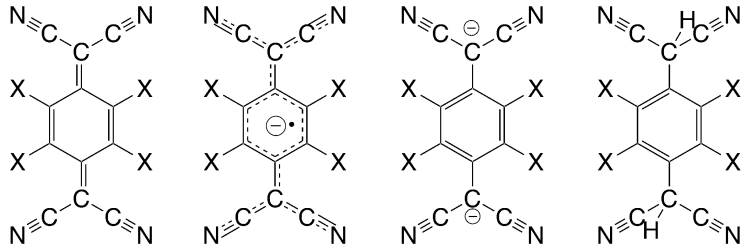

I **II** **III** **IV**

Scheme 1 Representations of X_4TCNQ in various oxidation and protonation states

In 2006, Kitagawa and co-workers described the generation of a coordination network in which sheets of $Zn(TCNQ^{II-})$ were linked by 4,4'-bipyridine ligands to create a porous coordination polymer, in which electron deficient guests were able to generate a colored material through interaction with the electron-rich $TCNQ^{II-}$ anion.[35] In this original work the $TCNQ^{II-}$ was formed serendipitously whilst in subsequent work, involving other divalent metal centers, $TCNQ^{II-}$ was deliberately generated using ascorbic acid as a reductant.[36] The color of the crystalline material obtained following adsorption of electron deficient guests depended not only on the nature of the guest but also the divalent metal from which the network was formed. This elegant work of Kitagawa and co-workers clearly demonstrated that the TCNQ dianion could serve as a donor in charge-transfer interactions in which it is a network component.

In this current work we describe a remarkable network material in which Mn(II) centers are linked by μ_4-F_4TCNQ^{II-} ligands and are coordinated by *trans* pyridine (py) ligands. The coordination polymer exhibits unusual flexibility arising from unprecedented rotation around

columns of face-to-face coordinated pyridine moieties, which act as pseudo-axles. In addition to the adsorption of CO_2 and CS_2 the uptake of various electron acceptors leads to a major structural transformation in addition to changes to the spectroscopic and electrical properties. The experimental work is complemented by periodic density functional theory (DFT) calculations that have been employed to rationalise the experimental observations and physical properties.

Experimental

Synthesis of $Mn(F_4TCNQ)(py)_2$·solvate

A solution of manganese nitrate hexahydrate (13.4 mg, 0.047 mmol) and pyridine (0.1 mL) in methanol (6 mL) was layered over F_4TCNQH_2 (13 mg, 0.047 mmol) in DMF (1 mL). The pale yellow crystals that formed were collected and air dried (17.5 mg, 0.033 mmol, 71%). Anal. Calcd for $[Mn(C_{12}N_4F_4)(C_5H_5N)_2]\cdot 0.25(H_2O)$: C, 53.51; H, 2.14; N, 17.02%. Found: C, 53.44; H, 2.62; N, 17.31%. Details relating to the generation of the closed channel crystals and the intercalated species are available in the Supporting Information (S1).

Crystallography

$[Mn(C_{12}F_4N_4)(C_5H_5N_1)_2]\cdot 2MeOH$, M_r = 553.38, monoclinic, *C2/m*, a = 15.502(2) Å, b = 7.3623(6) Å, c = 11.6926(10) Å, β = 102.666(11)°, V = 1302.0(2) Å^3, Z = 2, θ_{max} = 67.639°, CuK_α radiation, λ = 1.54184 Å, T = 130 K, pale yellow, μ = 4.671 mm^{-1}, ρ(calcd) = 1.412 g/cm^3, 2164 independent reflections. $wR2$(all data) = 0.1732 and $R1(I>2\sigma(I))$ = 0.0587. *Goodness of Fit* = 0.992.

$[Mn(C_{12}F_4N_4)(C_5H_5N_1)_2]$ (closed form), M_r = 489.30, orthorhombic, *Imma*, a = 22.109(4) Å, b = 7.3760(15) Å, c = 12.353(3) Å, V = 2014.5(7) Å^3, Z = 4, θ_{max} = 22.632°, synchrotron radiation, λ = 0.71080 Å, T = 100 K, pale yellow, μ = 0.715 mm^{-1}, ρ(calcd) = 1.613 g/cm^3, 677 independent reflections, $wR2$(all data) = 0.2682 and $R1(I>2\sigma(I))$ = 0.0881, *Goodness of Fit* = 1.147.

$[Mn(C_{12}F_4N_4)(C_5H_5N_1)_2].1.4CS_2$, M_r = 595.88, monoclinic, *C2/c*, a = 25.016(7), b = 7.3400(15) Å, c = 15.536(3) Å, β = 114.06(3)°, V = 2604.8(12) Å^3, Z = 4, θ_{max} = 24.997°, synchrotron radiation, λ = 0.71080 Å, T = 100 K, pale yellow, μ = 0.784 mm^{-1}, ρ(calcd) =

1.519 g/cm^3, 2256 independent reflections, *wR*2(all data) = 0.4878 and *R*1(*I*>2σ(*I*)) = 0.1600. *Goodness of Fit* = 2.416.

[Mn($C_{12}F_4N_4$)($C_5H_5N_1$)$_2$]·benzoquinone, M_r = 597.39, triclinic, *P-1*, *a* = 7.2950(13) Å, *b* = 8.493(2) Å, *c* = 11.722(2) Å, α = 74.39(2)°, β = 88.282(15)°, γ = 66.29(2)°, *V* = 637.9(3) Å^3, *Z* = 1, θ_{max} = 67.723°, CuK$_\alpha$ radiation, λ = 1.54184 Å, *T* = 130 K, blue, μ = 4.823 mm^{-1}, ρ(calcd) = 1.555 g/cm^3, 2120 independent reflections, *wR*2(all data) = 0.4021and *R*1(*I*>2σ(*I*)) = 0.1484, *Goodness of Fit* = 1.357.

[Mn($C_{12}F_4N_4$)($C_5H_5N_1$)$_2$]·maleic anhydride, M_r = 587.36, monoclinic, *C*2/*m*, *a* = 15.5820(6) Å, *b* = 7.3247(2) Å, *c* = 11.7312(5) Å, β = 103.712(4)°, *V* = 1300.76(9) Å^3, *Z* = 2, θ_{max} = 67.495°, Cu$_{K\alpha}$ radiation, λ = 1.54184 Å, *T* = 130 K, red, μ = 4.766 mm^{-1}, ρ(calcd) = 1.500 g/cm^3, 1263 independent reflections, *wR*2(all data) = 0.1925 and *R*1(*I*>2σ(*I*)) = 0.0706, *Goodness of Fit* = 1.074.

[Mn($C_{12}F_4N_4$)($C_5H_5N_1$)$_2$]·nitrobenzene, M_r = 612.41, monoclinic, *C*2/*m*, *a* = 15.6492(15) Å, *b* = 7.3327(4) Å, *c* = 11.6454(8) Å, β = 106.612(9)°, *V* = 1280.55(18) Å^3, *Z* = 2, θ_{max} = 67.492°, CuK$_\alpha$ radiation, λ = 1.54184 Å, *T* = 130 K, orange, μ = 4.832 mm^{-1}, ρ(calcd) = 1.588 g/cm^3, 1256 independent reflections, *wR*2(all data) = 0.2183 and *R*1(*I*>2σ(*I*)) = 0.0754, *Goodness of Fit* = 1.144.

[Mn($C_{12}F_4N_4$)($C_5H_5N_1$)$_2$]·I_2, M_r = 743.10, monoclinic, *C*2/*m*, *a* = 15.929(11) Å, *b* = 7.3947(18) Å, *c* = 11.505(7) Å, β = 107.66(7)°, *V* = 1291.3(13) Å^3, *Z* = 2, θ_{max} = 67.471°, CuK$_\alpha$ radiation, λ = 1.54184 Å, *T* = 130 K, black, μ = 23.390 mm^{-1}, ρ(calcd) = 1.911 g/cm^3, 1265 independent reflections, *wR*2(all data) = 0.5235 and *R*1(*I*>2σ(*I*)) = 0.2045, *Goodness of Fit* = 1.731.

Results and Discussion

The open and closed forms of Mn(F_4TCNQ)(py)$_2$

Reaction of manganese(II) nitrate with F_4TCNQH_2, (**IV**, X = F), and pyridine in MeOH/DMF generates crystals of solvated Mn(F_4TCNQ)(py)$_2$ suitable for single crystal X-ray diffraction analysis. The crystal structure determination reveals octahedral Mn(II) centers coordinated by *trans* pyridine ligands and four F_4TCNQ dianions. Each F_4TCNQ dianion is

bound to four crystallographically equivalent Mn(II) centers within a 2D network as indicated in Figure 1a. Whilst all Mn centers within the network are co-planar, the μ_4 dianions are not flat, with the aromatic ring, which is disordered over two sites, inclined to the mean plane of the network. The Mn(II) centers bound to a single F_4TCNQ dianion lie at the vertices of a rectangle with edges 7.3623(6) Å and 11.6926(10) Å. The pyridine rings are oriented around the Mn-N bond with their normals parallel with the short edges of the Mn_4 rectangles. This disposition allows pyridine rings from adjacent sheets to interdigitate snugly as indicated in Figure 1b. Columns of face-to-face pyridine units are thus generated which provide a crucial component of the unusual rearrangement process accompanying desolvation as described below. The separation of 7.3623(6) Å between manganese centers along the shorter edge of the Mn_4 rectangle is ideally suited to this interdigitation. Highly disordered solvent molecules are located within the channels that are apparent in Figure 1b. The form depicted in Figure 1 is herein referred to as the open form.

When a single crystal of solvated $Mn(F_4TCNQ)(py)_2$ is mounted on the diffractometer and gently heated under a stream of nitrogen, the crystal structure remains unchanged up to approximately 40 °C. Between 40 and 50 °C a major rearrangement accompanies the complete removal of solvent which occurs with retention of single crystal character. The original connectivity within the sheets is retained although there is a significant change in the sheet geometry as can be seen by comparison of Figure 1a with Figure 2a. In the extended structure of the desolvated crystal, the channels are absent as is apparent from inspection of Figure 2b. This form is herein referred to as the closed form.

a)

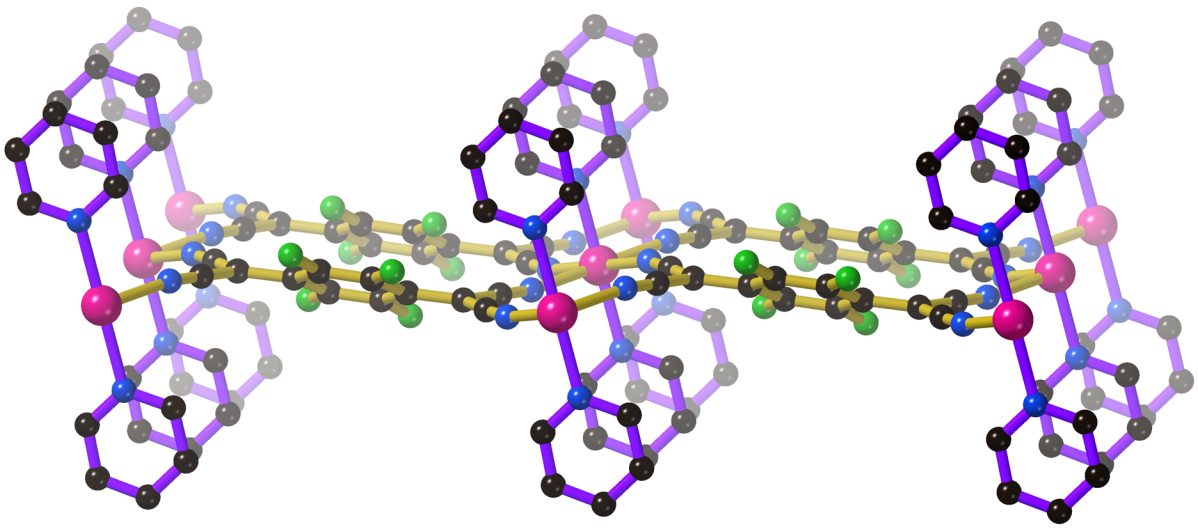

b)

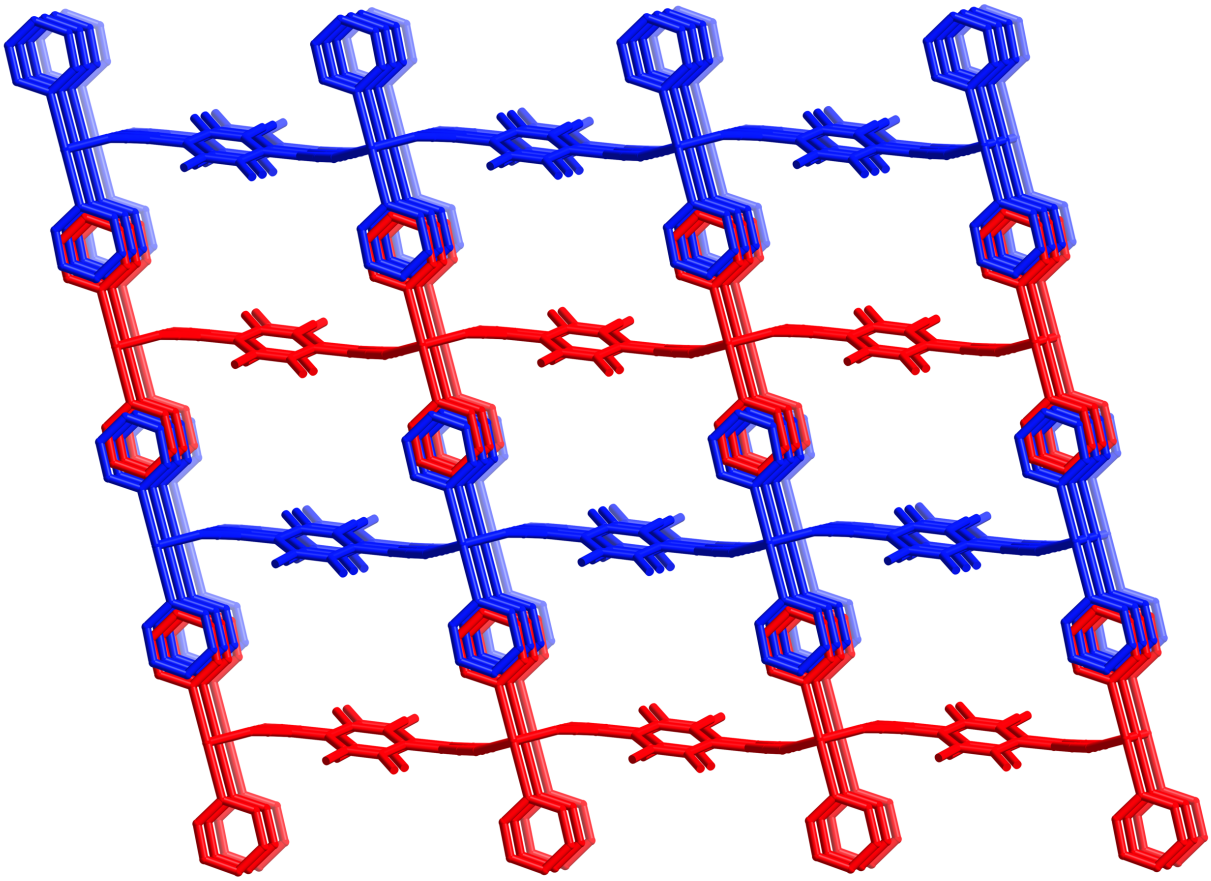

Figure 1. The structure of the framework in solvated $Mn(F_4TCNQ)(py)_2$. a) A single $Mn(F_4TCNQ)(py)_2$ sheet. The C_6F_4 rings are disordered over two orientations only one of which is shown here; Color code: Mn magenta, F green, N, blue, C black. b) Four sheets, illustrating the interdigitation of the pyridine units; columns of face-to-face pyridine units extend into the page. Hydrogen atoms have been omitted for clarity.

The conversion between the two forms would appear to require a concerted movement of the framework components as indicated in the animation which forms part of the Supporting Information. In the closed form (Figure 2b), F_4TCNQ^{2-} components are strongly bowed toward each other across what had been channels in the open form (Figure 1b). This creates a larger second type of channel which is filled by columns of face-to-face pyridine rings which have collapsed inwards, towards each other (Figure 2b). During the collapse the pyridine rings from one $Mn(F_4TCNQ)(py)_2$ sheet within a given column swivel through a considerable angle (~76°) relative to the pyridine rings from the other sheet (Figure S9). The angle between the py(N)···py(C4) vectors of neighbouring pyridine rings decreases from 180° in the open form

(where the vectors are parallel but point in opposite directions, as can be seen in Figure 1b) to 103.9° in the closed form (Figure 2b). A consequence of these rotations is that a marked contraction perpendicular to the sheets occurs; thus the Mn sheet-to-Mn sheet separation decreases by ~18% from 7.562 Å in the open form to 6.177 Å in the collapsed form.

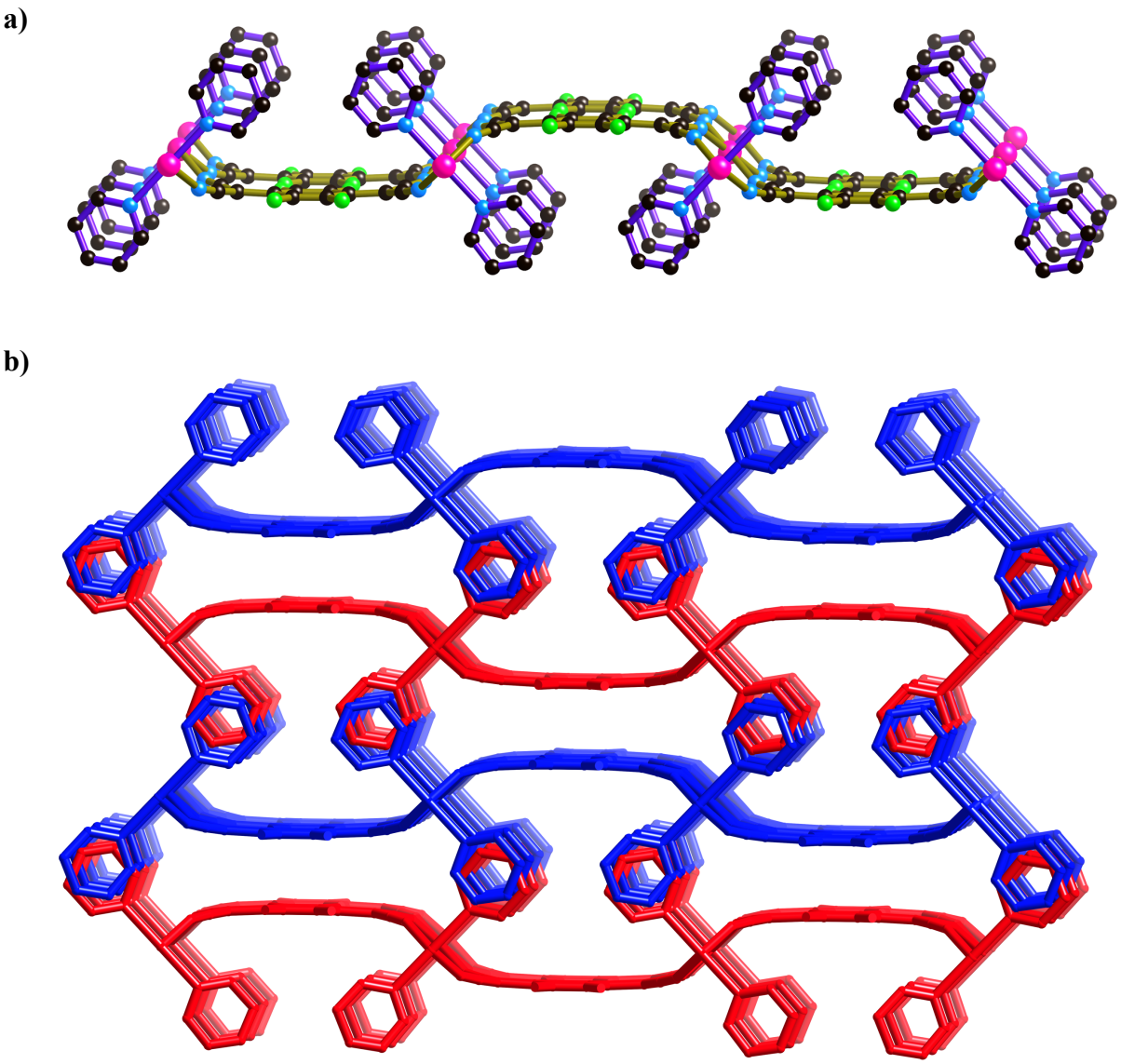

Figure 2. The structure of the desolvated, closed form of $Mn(F_4TCNQ)(py)_2$. a) A single $Mn(F_4TCNQ)(py)_2$ sheet; pyridine ligands are indicated by purple bonds. Color code as for Figure 1a. b) Four sheets, illustrating the interdigitation of the pyridine units; columns of face-to-face pyridine units extend into the page. Hydrogen atoms have been omitted for clarity.

Attention has previously been drawn to the pronounced flexibility of the $M_4(TCNQ^{II-})$ system in which each of the four C-CN arms is attached to a metal center.[33] Variations in bond angles of only a few degrees at the atoms in each arm are sufficient to generate very different geometrical dispositions of the four attached metal centers. A comparison of Figure 1a and 2a reveals two very different sets of positions of the metal centers bound to the F_4TCNQ dianion. In Figure 1a, it is apparent that two metal centers lie on each side of the mean plane of the dianion, whereas in Figure 2a all four metal centers are located on the same side of the μ_4 ligand. A contraction in Mn···Mn separation (~5%) along the longer edge of the Mn_4 rectangle accompanies desolvation. It is significant that, despite the marked contractions perpendicular to the sheets as well as within the sheets, the py···py separations within the intact columns remain unchanged.

The contraction process whereby face-to-face contact of the pyridine rings remains in place while the relative orientation of adjacent rings changes by 76° constitutes a unique and dynamic structural feature. We are not aware of any previous report of a mode of large-scale molecular movement of this type; its essence is the rotation of flat aromatic components relative to their immediate neighbours, with which they are in close π-to-π contact, within an extended, face-to-face, column. It differs fundamentally from the usual modes of framework flexibility involving changes in bond angles or rotations around covalent or coordinate bonds.

The result of the above molecular movements is that the volume of the framework contracts remarkably during the collapse to 77.3% of the initial, and the process is readily reversed as described below.

Adsorption of guests by $Mn(F_4TCNQ)(py)_2$

The structural flexibility exhibited by $Mn(F_4TCNQ)(py)_2$ upon loss of solvent molecules raised the prospect that the structural changes could be reversed upon adsorption of appropriate guests. In this section the adsorption investigations relating to a variety of guests are described. The initial adsorption studies focus on the uptake of common gasses and volatile compounds whilst later investigations are directed towards the incorporation of guests that can serve as electron acceptors in charge transfer interactions with the electron-rich framework.

Adsorption measurements were undertaken on the closed form of $Mn(F_4TCNQ)(py)_2$ which had undergone desolvation at 40 °C under vacuum. The uptake of H_2 was measured at

77 K but even up to a pressure of 2500 kPa, no H_2 adsorption was recorded. A negligible level of nitrogen was adsorbed up to 100 kPa at 77 K and similarly, at a temperature of 298 K no nitrogen was adsorbed even up to a pressure approaching 3,000 kPa. Adsorption measurements with CH_4 performed at 258 K and up to 3000 kPa also failed to indicate any significant level of adsorption. Isotherms associated with these adsorption measurements are presented in the SI, section 7.

The adsorption of CO_2 by samples of the closed form of $Mn(F_4TCNQ)(py)_2$ (previously desolvated at 40 °C under vacuum) shows unusual features (Figures 3 and S15) consistent with a process in which the initial structure, devoid of pores, opens up under the influence of the CO_2 - the reverse of the collapse process described above. At 298 K negligible sorption occurs below *ca.* 500 kPa but between ca. 800 and 1000 kPa the isotherm, sigmoidal in shape, becomes much steeper. The isotherm plateaus at pressures above 1000 kPa with an overall uptake at room temperature of ~130 milligrams of CO_2 per gram of sorbent; this corresponds to approximately 1.5 mols of CO_2 per $Mn(F_4TCNQ)(py)_2$ formula unit. Marked hysteresis is observed upon desorption. The complete reversibility of the adsorption/desorption cycle was demonstrated by using the *same* sample for repeated CO_2 sorption measurements at different temperatures (298, 273 and 258 K), each sorption step being followed by desorption. At a given temperature, essentially identical isotherms were reproducibly observed after numerous cycles. At lower temperatures, "saturation" of the sample occurs at pressures lower than those required at 298 K and the hysteretic loop of the isotherms is narrowed. Significantly, single crystal X-ray diffraction analysis of an individual crystal selected from a bulk sample that had been subjected to CO_2 adsorption and then to desorption under vacuum, reveals a return to the closed structure seen in Figure 2; powder XRD of the bulk sample treated to the same cycle also indicates the collapsed structure (Figure S2). An *in situ* powder diffraction investigation supported the structural changes occurring upon CO_2 adsorption and desorption (see SI). The fact that negligible sorption of CO_2 occurs until a certain threshold CO_2 pressure is applied and then the amount adsorbed increases sharply with increasing pressure, is consistent with the view that significant CO_2 pressure is required before the collapsed structure starts to rearrange to the open structure, which then readily adsorbs further CO_2. Similar CO_2 adsorption behaviour has been interpreted previously in terms of structural changes induced by the incoming gas facilitating further gas uptake.[37, 38]

Although it was not possible to obtain single crystal X-ray diffraction data that reveals the position and orientation of adsorbed CO_2, we were able to incorporate the close relative, CS_2, into $Mn(F_4TCNQ)(py)_2$, and determine its location and orientation. Crystals of the closed form of $Mn(F_4TCNQ)(py)_2$ underwent a single crystal-to-single crystal transformation upon soaking in liquid carbon disulfide, to yield $[Mn(F_4TCNQ)(py)_2]\cdot 1.4(CS_2)$. X-ray diffraction revealed that the framework had been transformed from the initial closed form to the open form, with CS_2 molecules within the channels (1.4 CS_2 per Mn), as shown in Figure 4. The CS_2 molecules are disordered over two positions. One end of the CS_2 molecule makes close contact with a pyridyl unit ($S\cdots\beta C_{pyr}$, 3.18 Å and $S\cdots\beta H_{pyr}$, 2.94 Å) and also with the aromatic ring of the F_4TCNQ^{2-} ligand. The fact that the framework adsorbs 1.5 - 1.6 molecules of CO_2 and only slightly less (1.4) CS_2 molecules per metal center suggests that the CO_2 may associate with the framework in a similar manner.

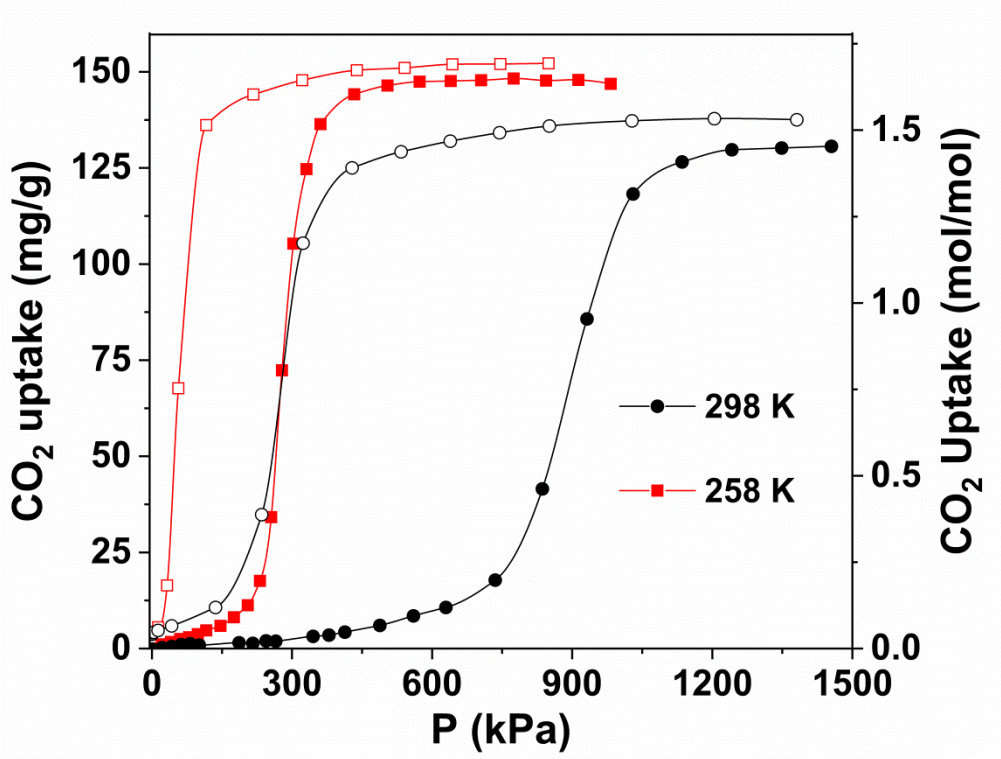

Figure 3. CO_2 sorption/desorption by $Mn(F_4TCNQ)(py)_2$ at 298 K (black markers) and 258 K (red markers). The filled markers correspond to adsorption isotherms, whilst unfilled markers correspond to desorption isotherms.

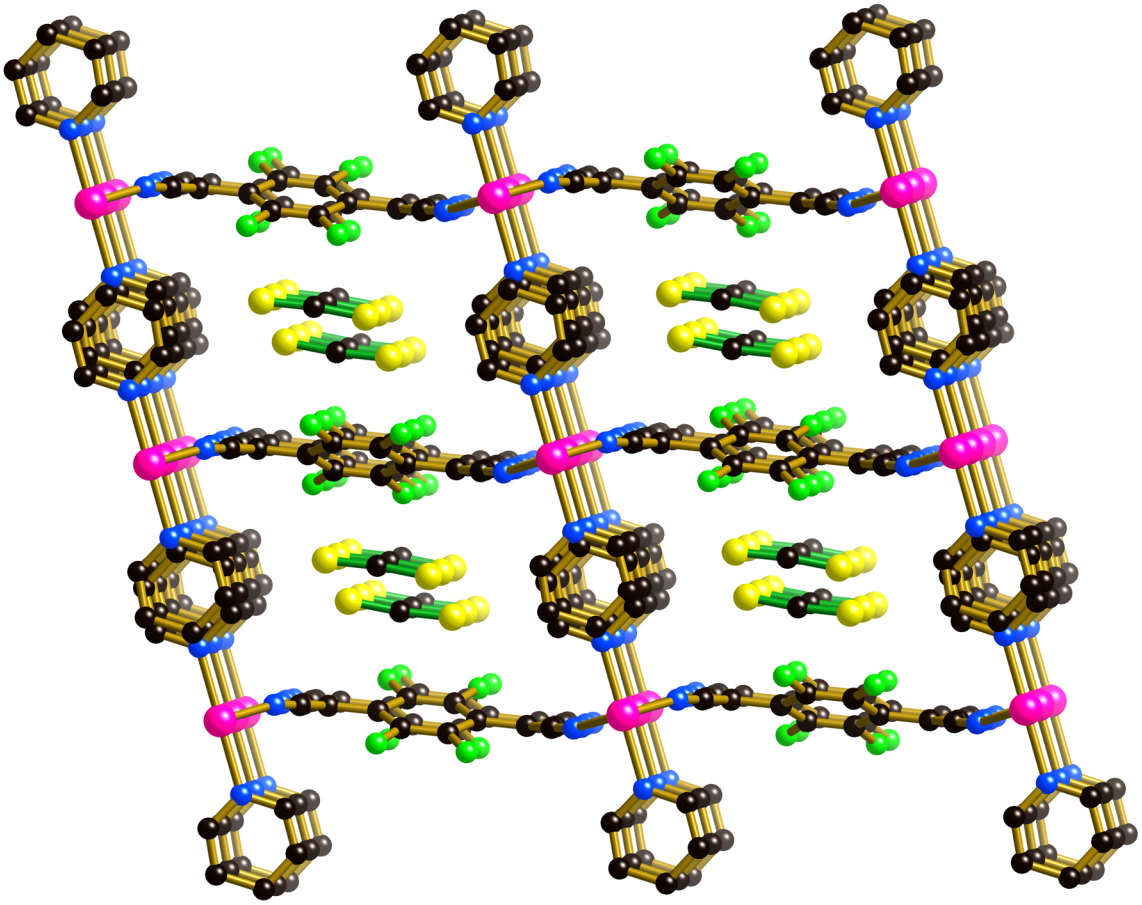

Figure 4. The structure of $[Mn(F_4TCNQ)(py)_2]\cdot 1.4(CS_2)$. The CS_2 molecules are shown with green bonds. H atoms have been omitted for clarity.

The pore opening process within crystals of $[Mn(F_4TCNQ)(py)_2]$ is triggered by the incorporation of guest species but the adsorption study indicates that not all small molecules are capable of inducing the structural changes necessary for adsorption. It is proposed that the structural rearrangements that occur in response to adsorption and desorption of guest molecules reflect a strong tendency of F_4TCNQ^{2-} ligands to associate with molecules on their delocalised π-surfaces. The structure determination of the solvated form of the crystal clearly shows electron density consistent with disordered solvent molecules making close contact with the π-surfaces. If a structural rearrangement was not possible, then the loss of the volatile methanol molecules would lead to empty channels with exposed F_4TCNQ^{2-} surfaces. The collapse of the channels allows close approach of π-surfaces from a neighbouring F_4TCNQ^{2-}

ligand on one side of each F_4TCNQ^{2-} ligand and C-H hydrogen atoms from coordinated pyridyl groups on the other, thus ensuring no bare surfaces. It is this association that is responsible for the buckling of the Mn(F_4TCNQ) network and the relative rotation of adjacent pyridine ligands in the face-to-face stacks (Figure 2). The failure of [Mn(F_4TCNQ)(py)$_2$] to adsorb H_2, N_2 or CH_4 under conditions which include pressures approaching 3,000 kPa, reflects the relatively weak attraction of these molecules for the internal pore surfaces of the coordination polymer. Binding energies for H_2, N_2 or CH_4 with porous coordination polymers are generally low and commonly in the range of 5-10, 8-20 and 15-25 kJmol^{-1} [39-41] respectively, indicating the relatively weak association between these species and typical host networks. Binding enthalpies for CO_2 are in general, significantly higher (20-30 kJmol^{-1})[39] and thus a stronger van der Waals interaction may be anticipated between the F_4TCNQ surfaces and CO_2. The sigmoidal isotherms suggest that the pore opening process only begins when the pressure of CO_2 is great enough for the CO_2 to force its way into the closed pores thus separating the framework surfaces and initiating the concerted pore opening process throughout the crystal. At this point a cooperative effect is apparent as pore expansion, akin to a gate opening process, facilitates the incorporation of further CO_2 molecules and this is the reason for the steepness of the isotherm. The expansion of the framework to a larger, open pore structure as the CO_2 pressure is increased may at first seem counterintuitive but it is the increased availability of CO_2 molecules at high pressure which drives the incorporation of CO_2 into the crystalline network material.

As indicated above, previous structural work with metal derivatives of F_4TCNQ^{2-} and $TCNQ^{2-}$ has demonstrated that changes in the angle at the coordinating nitrogen of just a few degrees can lead to very different geometrical arrangements.[33] It is noted that the change in the angle at the coordinating nitrogen allows a major reorientation of half of the Mn(II) octahedral geometries and a relatively minor reorientation of the other half, as indicated in Figure S9 (SI). Accompanying the change in angle at the coordinating nitrogen is the relative rotation of the aromatic rings that occurs in the parallel columns of face-to-face pyridines. The swivelling around an axis that passes through the faces of interdigitating pyridines proceeds with face-to-face contact being maintained throughout a rotation of 76°. Such a transition, which is pivotal to the large geometric rearrangement that occurs, would appear to be possible because the nature and extent of the face-to-face π-interactions between the components is not significantly altered throughout the transition process. Although the transitions from the open to the closed

form and vice versa, represent major structural changes, the energy cost associated with both changing the angle at the coordinating nitrogen and rotating the pyridine groups would appear to be relatively small. It is therefore not surprising that incorporation of a guest, with sufficient affinity for the pore surfaces, is able to drive the host structure from the closed to the open form.

Adsorption of electron acceptors by $Mn(F_4TCNQ)(py)_2$ and the effects of charge-transfer interactions on electronic properties

The adsorption investigations with CO_2 and CS_2 clearly demonstrate the flexibility of the $Mn(F_4TCNQ)(py)_2$ as indicated by the switch from the closed form to the open form resulting from the association of guest molecules with the host network. These results prompted further exploration of host-guest association to determine if electron deficient guests would be able to form charge-transfer interactions with the electron-rich F_4TCNQ dianions of the networks and trigger the opening of the closed channels in a similar manner to CO_2 and CS_2.

Pale yellow $Mn(F_4TCNQ)(py)_2$ crystals on exposure to vapors of the electron acceptors, nitrobenzene, maleic anhydride, benzoquinone and iodine become deeply colored as the molecules are adsorbed into the framework. Upon adsorption of the yellow benzoquinone, the pale yellow crystals become a vivid blue, with maleic anhydride they turn a vibrant red and the inclusion of nitrobenzene results in a bright orange. In the case of adsorption of iodine the crystals become essentially jet black. Photographs indicating the dramatic color changes associated with the incorporation of the electron deficient guests are presented in the Supporting Information. The color change is indicative of charge transfer interactions between the e^--donor F_4TCNQ^{2-} components of the host network and the electron-accepting intercalant. It was possible to carry out X-ray diffraction measurements on single crystals of these adducts which clearly revealed the framework was present in its open form.

Only in the case of the benzoquinone was the intercalant found to be ordered. A view of the structure of the benzoquinone adduct is presented in Figure 5. There is one benzoquinone molecule per Mn and only one orientation of the C_6F_4 rings is apparent. The location and orientation of the benzoquinone intercalant are well defined. The quinonic oxygen atoms make close contacts with the non-fluorinated C atoms of the C_6F_4 rings (O···C, 3.149 Å) and also with C atoms of the pyridyl columns (C···O, 3.039 and 3.327 Å.). In addition, the CH moieties

of the benzoquinone interact significantly with the nearby F_4TCNQ^{2-} ligands. Benzoquinone appears to fit rather snugly into the channels and it is perhaps not surprising that bulkier electron acceptors such as chloranil failed to intercalate, as evident by lack of colour change when exposed to vapors of the acceptor.

Whilst diffraction data on the nitrobenzene, maleic anhydride and iodine adducts failed to yield the molecular structure of the intercalated guest, residual electron density within the channels of the open form of the structure are consistent with the inclusion of the respective guests. Using the SQUEEZE routine within PLATON[42] the number of nitrobenzene, maleic anydride and I_2 molecules per Mn(II) were estimated to be 0.9, 1.2 and 1.2 respectively.

Infrared spectra are consistent with the inclusion of the intercalant into the framework structure. Of particular importance are the ν(CN) bands which provide a useful indication of the oxidation state of the F_4TCNQ moiety. The ν(CN) frequencies observed for the solvated open form, the desolvated closed form and the adducts with nitrobenzene, maleic anhydride, benzoquinone and iodine are remarkably invariant (2198±2, 2153±1, 2128±2 cm^{-1}), and are consistent with other examples involving coordinated F_4TCNQ^{2-}.[28]

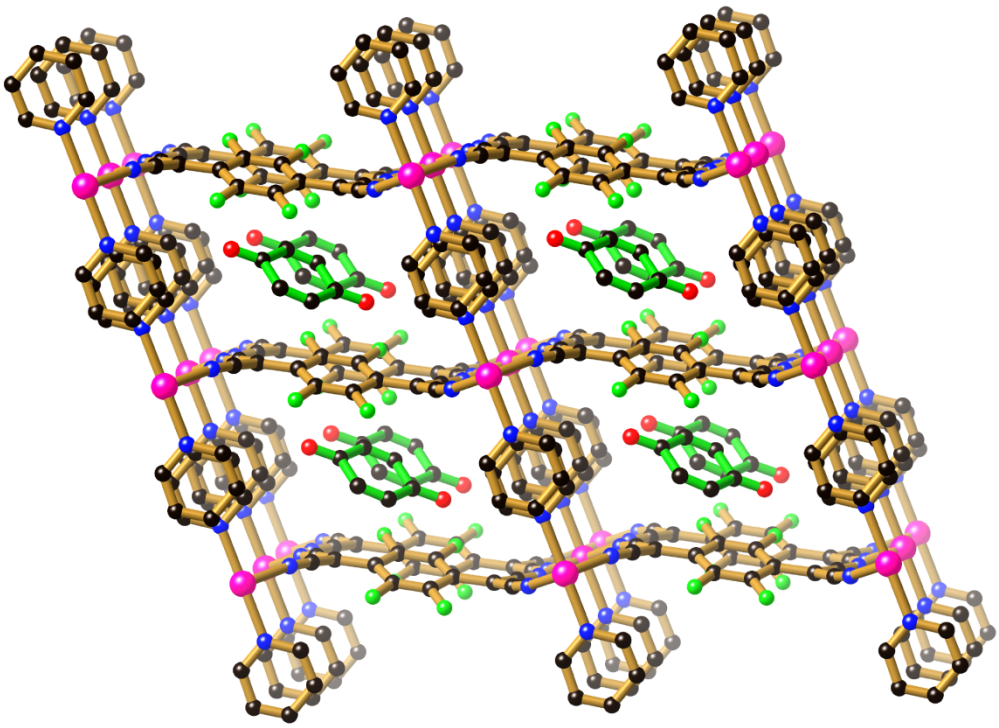

Figure 5. The structure of $Mn(F_4TCNQ)(py)_2 \cdot$benzoquinone.The benzoquinone molecules are indicated with green bonds. H atoms have been omitted for clarity.

As can be seen in Figure 6, the vis-NIR spectra of $Mn(F_4TCNQ)(py)_2$, in both open and closed forms, shows little absorption in the observed 5000-25000 cm^{-1} range, whereas the adducts with electron accepting guests show significantly enhanced absorption, which is attributed to charge-transfer interactions between the donor F_4TCNQ^{2-} components of the framework and the acceptor intercalants. The absorption tails of the adducts extend further towards the infrared region in the following order for the intercalants: nitrobenzene, maleic anhydride, benzoquinone and iodine.

The optical band gaps of the adducts, calculated from Tauc plots,[43] appear to exhibit a dependence on the electron affinity of the intercalants; the higher the electron affinity the smaller the optical band gap (Figure 7). The approximate linear dependence on electron affinity points to the opportunity to 'tune' the optical bandgap of $Mn(F_4TCNQ)(py)_2$ adducts through intercalation.

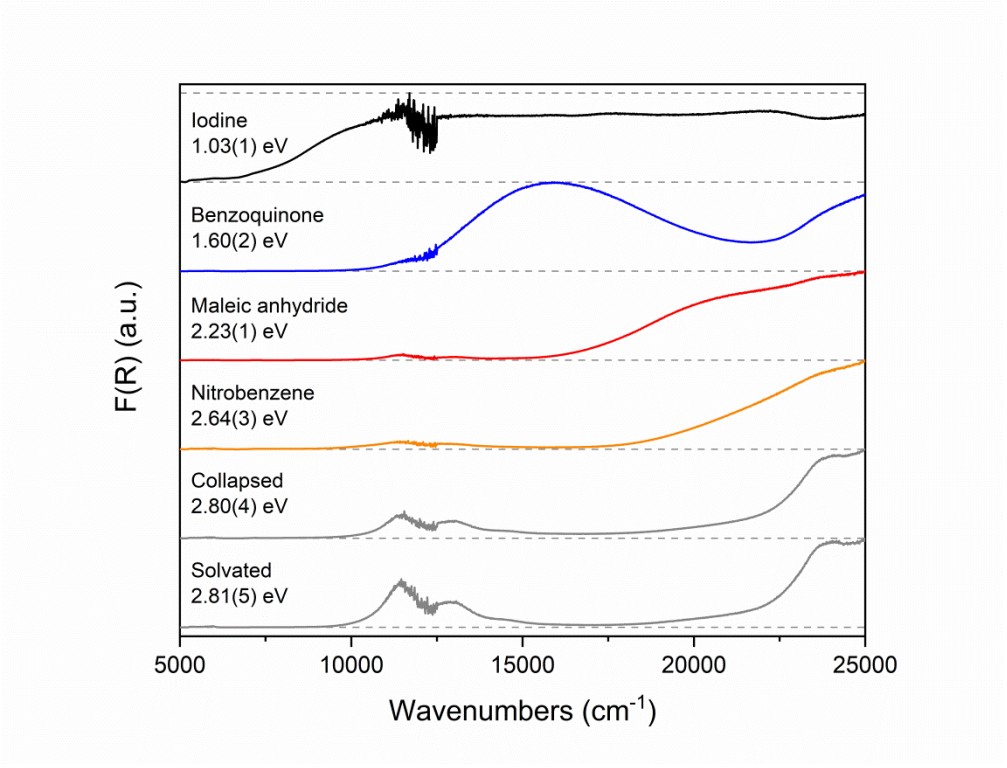

Figure 6. Visible/NIR spectra of $Mn(F_4TCNQ)(py)_2$ (in both open and closed forms) and the adducts with nitrobenzene, maleic anhydride, benzoquinone and I_2. Optical bandgaps for each sample are also disclosed (Tauc plots are available in the Supporting Information).

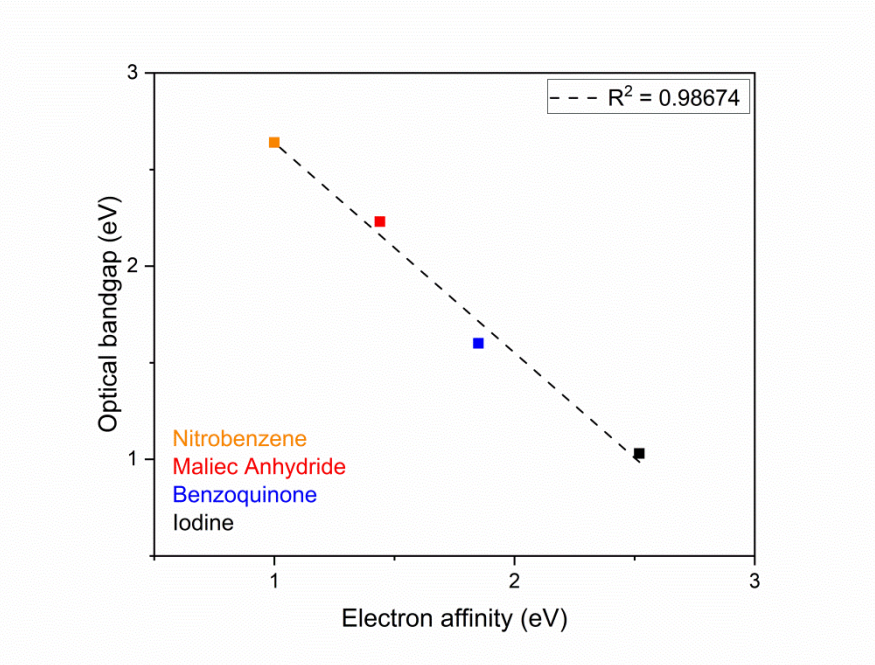

Figure 7. The optical band gaps of the adducts vs the electron affinity of the intercalants.

In the expectation that a reduction in the optical band gap would be accompanied by an increase in electrical conductivity, we investigated the variation in conductivity of $Mn(F_4TCNQ)(py)_2$ as the vapors of the electron acceptors nitrobenzene, maleic anhydride, benzoquinone and iodine were diffused into the solid. Interdigitating electrodes were used for this purpose, as they allow conductivity to be monitored as the sorption proceeds. Under a nitrogen atmosphere, shielded from light and held at 295 K, $Mn(F_4TCNQ)(py)_2$ in the closed form was found to have a conductivity of ~ 5 x 10^{-10} S/cm. Adsorption of the above electron acceptors increases the conductivity (Figure 8); the higher the electron affinity of the intercalant, the greater the conductivity, a trend similar to that observed for the optical bandgaps. A plot of $ln(\sigma/\sigma_0)$ vs E_A is presented in the supporting information (Figure S29). The strongest electron acceptor, I_2, leads to a pronounced increase in conductivity of nearly five orders of magnitude (1.4 x 10^{-4} S/cm).

With the intention of exploring the relationship between the observed optical and electrical properties and electron affinity upon intercalation, solid-state DFT calculations at the PBE[44]//PBE-D3(BJ)[45] level of theory were carried out for the closed $Mn(F_4TCNQ)(py)_2$ framework and for the benzoquinone adduct. The benzoquinone adduct was selected because the location of the intercalant is clearly indicated by the crystallographic investigation.

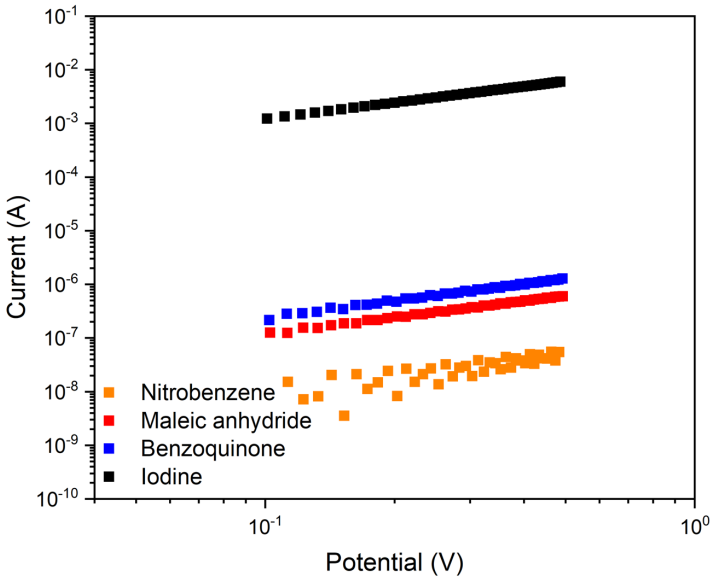

Figure 8. I-V curves of the $Mn(F_4TCNQ)(py)_2$ framework prior to and after exposure to electron acceptors.

The spin-polarized band structures and density of states plots (DOS) for the 'closed' $Mn(F_4TCNQ)(py)_2$ structure and the 'open' $[Mn(F_4TCNQ)(py)_2]\cdot$benzoquinone structure are presented in the supporting information (Figures S31-S34). For the 'closed' $Mn(F_4TCNQ)(py)_2$ structure, both spin channels of the valence band are largely comprised of Mn *d* orbitals, with N *p* orbitals and C *p* orbitals of the F_4TCNQ^{2-} ligands making minor contributions to the valence band (see Figure 9b). The conduction band of the closed form consists largely of *p* orbitals belonging to the coordinated pyridine ligands (Figures 9a).

Despite significant structural change upon intercalation of the electron acceptor, 1,4-benzoquinone, there does not appear to be a significant change to the composition of the valence band (comparison of Figures 9b and 9d). There is, however, a significant change to the conduction band upon intercalation. The composition of the conduction band is altered and consists only of *p* orbitals belonging to C and O atoms of the 1,4-benzoquinone (Figure 9c) and is lower in energy than the conduction band of the closed form. The enhanced conductivity that occurs upon intercalation may be explained by the conduction band moving closer in energy to the valence band. Similarly, the decrease in optical band gap may be attributed to the presence of a lower energy conduction band upon intercalation.

In order to rationalize the relationship between electron affinity and both optical band gap and conductivity it is useful to consider the energy diagram presented in Figure 10. The bandgap (E_G) is considered to be the difference in energy between the conduction band (CB) and the valence band (VB), whereas the electron affinity (E_A) is the difference between the vacuum energy (E_{Vac}) and the conduction band. The ionisation energy (I_E) is the difference between the valence band and the vacuum energy. When intercalation of a guest occurs, the bandgap is decreased if the electron affinity of the intercalant is greater than the electron affinity of the $Mn(F_4TCNQ)(py)_2$ framework. Given that the DFT calculations indicate that the valence band has similar energies in the closed and open forms, I_E may be considered to be the same in both the open and closed forms. Accordingly, there is a linear relationship between the electron affinity of the intercalant and the band gap ($E_A = I_E - E_G$) as long as the E_A of the intercalant is greater than that of the $Mn(F_4TCNQ)(py)_2$ framework and less than I_E. This explains the almost linear relationship between the optical band gap and E_A.

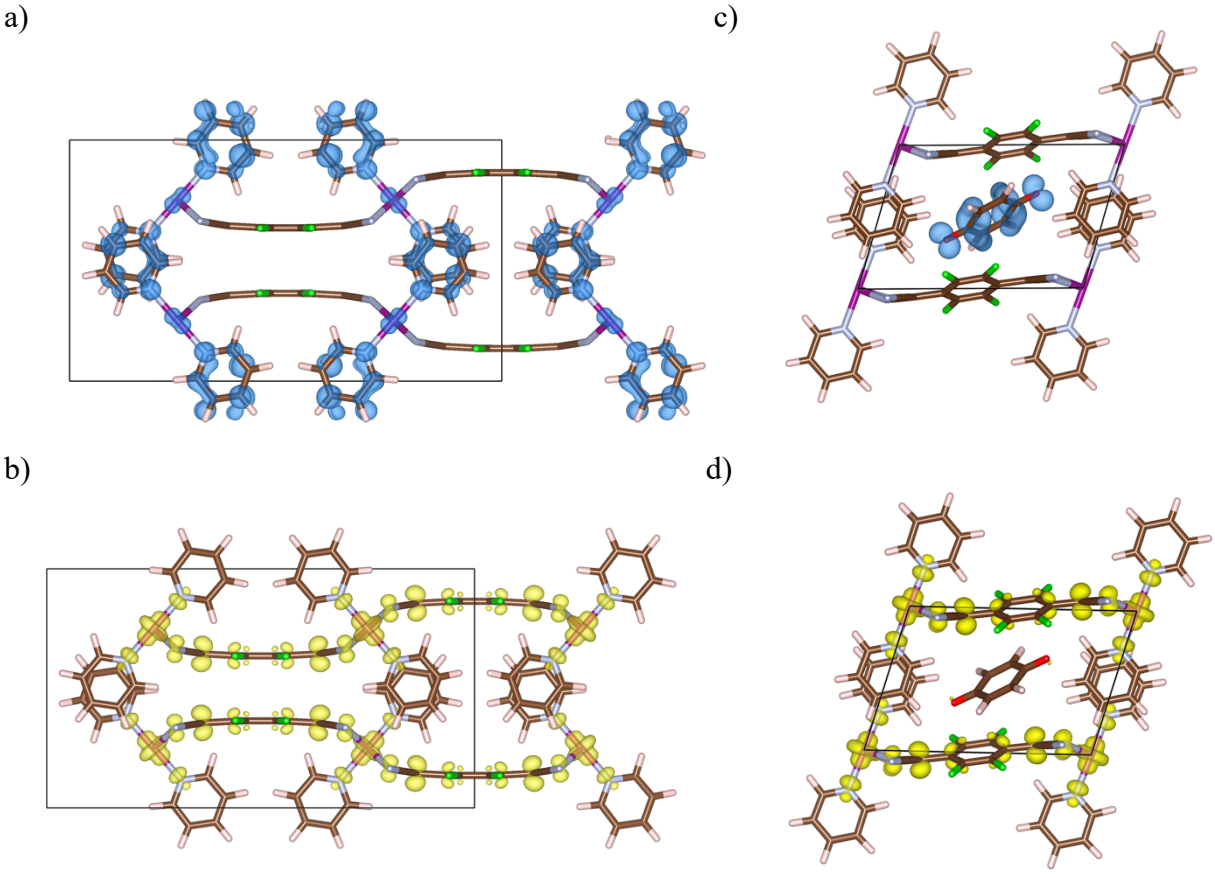

Figure 9. Band decomposed charge density plots of the closed $Mn(F_4TCNQ)(py)_2$ framework (a [conduction] & b [valence]) and the $[Mn(F_4TCNQ)(py)_2]\cdot$benzoquinone adduct (c [conduction] & d [valence]).

The DFT analysis also provides a rationalization for the trend in electrical conductivity i.e. the increase in conductivity with the increasing electron affinity of the intercalant. The relationship between conductivity and activation energy (E_a) for a semiconductor may be represented by the equation, $\sigma = \sigma_0 \exp\left(\frac{-E_a}{k_B T}\right)$ and given that $E_a \propto E_G$, then a linear relationship may be expected between ln(σ) and E_A. These relationships have important implications because it means that if a guest molecule can be intercalated into the Mn(F_4TCNQ)($py)_2$ framework then it may be possible to simply estimate the intercalant's electron affinity either by determining the optical band gap or measuring the electrical conductivity and using the respective plots as calibration graphs.

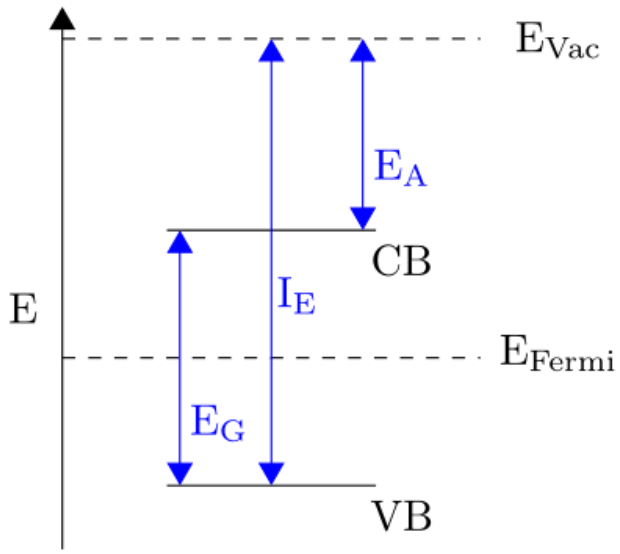

Figure 10. Schematic representation of a band structure, indicating the relative energies of the valence band (VB), conduction band (CB), vacuum energy (E_{Vac}), ionisation energy (IE) and electron affinity (E_A).

Concluding remarks

In summary, an unprecedented mode of large-scale molecular movement, which enables the framework to switch between the open and closed forms, is provided by the columns of face-to-face pyridine units, within which sliding rotation of every pyridine ring relative to its two near neighbours through a large angle (~76°) occurs whilst π-π contact is maintained. Mn(F_4TCNQ)($py)_2$ adsorbs CO_2, showing a sigmoidal isotherm indicative of a sorption process wherein the initial dense, closed structure requires significant CO_2 pressure

before it rearranges to the open structure, which then readily adsorbs further CO_2. The framework reversibly cycles between open and closed forms as CO_2 is adsorbed and desorbed. Whilst there has been considerable work devoted to the gas adsorption properties of coordination polymers, much of the early emphasis was directed towards increasing the quantity of gas that could be adsorbed. With the evolution of the field of porous coordination networks there has been increasing interest in materials that are able to discriminate between guests and offer some degree of selectivity in the adsorption process, particularly those that are capable of network flexibility.[46,47] In this current work the amount of CO_2 that can be adsorbed may only be modest but its role in initiating an unprecedented pore opening mechanism offers considerable scope for selective gas adsorption. There would appear to be potential for exploiting a similar mechanism involving interdigitating aromatic groups in other systems. Indeed, it may prove possible to deliberately incorporate interdigitating aromatic groups into new coordination networks with the aim of producing materials that can easily and reversibly switch from open to closed forms in response to chemical or physical stimuli.

Pale yellow $Mn(F_4TCNQ)(py)_2$ adsorbs the e^--acceptors nitrobenzene, maleic anhydride, benzoquinone and iodine which participate in donor-acceptor interactions with the e^--donor F_4TCNQ^{2-} components of the framework to form deeply coloured adducts. In the case of the vibrant blue benzoquinone adduct, details of the location and orientation of the intercalant were obtained but the other *e*-acceptor intercalants were highly disordered. Of particular interest was the observation that optical band gaps decreased in an approximately linear manner with increasing electron affinity of the intercalant. Similarly, electrical conductivities of the adducts, which showed semiconductor behaviour, increased with increasing electron affinity of the intercalant, the iodine adduct showing an increase of almost five orders of magnitude. DFT calculations provide a rationale for the relationships between the electron affinities of the intercalants and both the optical band gaps and the electrical conductivities. It is proposed that the electron affinity of an intercalant can be estimated from determination of an optical band gap or measurement of electrical conductivity.

The enhancement of electrical conductivity upon incorporation of electron deficient guests is not simply a case of doping but rather represents a situation in which there are fundamental changes in the electrical and spectroscopic properties. The introduction of electron deficient guest molecules that participate in charge-transfer interactions provides a new pathway for electrical conduction. Furthermore, there would appear to be excellent prospects

for tuning the electrical conductivity of this material by selecting intercalants based on their electron affinity.

The remarkable flexibility of $Mn(F_4TCNQ)(py)_2$, leading to reversible channel opening processes upon exposure to certain vapors, has resulted in a material that not only exhibits selectivity in guest uptake but also significant changes in electrical and spectroscopic properties when electron acceptor guests are adsorbed. The work highlights opportunities for developing new families of multi-functional materials in which electroactive bridging ligands, exhibiting a degree of geometrical flexibility at the donor atom sites, are able to form network materials on combination with appropriate metal centers.

Associated Content

Supporting Information

The Supporting Information is available free of charge at https://pubs.acs.org/doi/10.1021/acs.inorgchem*******. Synthetic details, X-ray diffraction procedures and data, structural figures, thermogravimetric analysis, gas adsorption details, electron affinities of intercalants, crystal photographs, infrared spectra, UV-Vis-NIR spectra, electrical conductivity information, computational details, structural conversion animation.

Acknowledgements

The support of the Australian Research Council is gratefully acknowledged (DP150100570, FT170100283 and DP180101413). RWE and ALS thank the Australian Government for an Australian Postgraduate Award. This research was undertaken with the assistance of resources and services from the National Computational Infrastructure (NCI), within the National Computational Merit Allocation Scheme (project fk5). Part of this work was undertaken on the MX1 and Powder Diffraction Beamlines at the Australian Synchrotron.

References

1. Li, B.; Wen, H. M.; Cui, Y.; Zhou, W.; Qian, G.; Chen, B., Emerging Multifunctional Metal-Organic Framework Materials. *Adv Mater.* **2016,** *28* (40), 8819-8860.
2. Li, J. R.; Kuppler, R. J.; Zhou, H. C., Selective gas adsorption and separation in metal-organic frameworks. *Chem. Soc. Rev.* **2009,** *38*, 1477-1504.
3. Shimomura, S.; Higuchi, M.; Matsuda, R.; Yoneda, K.; Hijikata, Y.; Kubota, Y.; Mita, Y.; Kim, J.; Takata, M.; Kitagawa, S., Selective sorption of oxygen and nitric oxide by an electron-donating flexible porous coordination polymer. *Nat. Chem.* **2010,** *2*, 633-637.
4. Sun, L.; Campbell, M. G.; Dinca, M., Electrically Conductive Porous Metal-Organic Frameworks. *Angew. Chem. Int. Ed. Engl.* **2016,** *55*, 3566-3579.
5. Xie, L. S.; Sun, L.; Wan, R.; Park, S. S.; DeGayner, J. A.; Hendon, C. H.; Dinca, M., Tunable Mixed-Valence Doping toward Record Electrical Conductivity in a Three-Dimensional Metal-Organic Framework. *J. Am. Chem. Soc.* **2018,** *140*, 7411-7414.
6. Su, J.; Hu, T. H.; Murase, R.; Wang, H. Y.; D'Alessandro, D. M.; Kurmoo, M.; Zuo, J. L., Redox Activities of Metal-Organic Frameworks Incorporating Rare-Earth Metal Chains and Tetrathiafulvalene Linkers. *Inorg. Chem.* **2019,** *58*, 3698-3706.
7. Ma, L.; Abney, C.; Lin, W., Enantioselective catalysis with homochiral metal-organic frameworks. *Chem. Soc. Rev.* **2009,** *38*, 1248-56.
8. Hasegawa, S.; Horike, S.; Matsuda, R.; Furukawa, S.; Mochizuki, K.; Kinoshita, Y.; Kitagawa, S., Three-dimensional porous coordination polymer functionalized with amide groups based on tridentate ligand: selective sorption and catalysis. *J. Am. Chem. Soc.* **2007,** *129*, 2607-14.
9. Sawaki, T.; Aoyama, Y., Immobilization of a Soluble Metal Complex in an Organic Network. Remarkable Catalytic Performance of a Porous Dialkoxyzirconium Polyphenoxide as a Functional Organic Zeolite Analogue. *J. Am. Chem. Soc.* **1999,** *121*, 4793-4798.
10. van Koeverden, M. P.; Abrahams, B. F.; D'Alessandro, D. M.; Doheny, P. W.; Hua, C.; Hudson, T. A.; Jameson, G. N. L.; Murray, K. S.; Phonsri, W.; Robson, R.; Sutton, A. L., Tuning Charge-State Localization in a Semiconductive Iron(III)–Chloranilate Framework Magnet Using a Redox-Active Cation. *Chem. Mater.* **2020,** *32*, 7551-7563.
11. Darago, L. E.; Aubrey, M. L.; Yu, C. J.; Gonzalez, M. I.; Long, J. R., Electronic Conductivity, Ferrimagnetic Ordering, and Reductive Insertion Mediated by Organic

Mixed-Valence in a Ferric Semiquinoid Metal-Organic Framework. *J. Am. Chem. So.c* **2015,** *137*, 15703-15711.

12. Carrington, E. J.; McAnally, C. A.; Fletcher, A. J.; Thompson, S. P.; Warren, M.; Brammer, L., Solvent-switchable continuous-breathing behaviour in a diamondoid metal-organic framework and its influence on CO_2 versus CH_4 selectivity. *Nat. Chem.* **2017,** *9*, 882-889.
13. Kim, H. C.; Huh, S.; Lee, D. N.; Kim, Y., Selective carbon dioxide sorption by a new breathing three-dimensional Zn-MOF with Lewis basic nitrogen-rich channels. *Dalton Trans.* **2018,** *47*, 4820-4826.
14. Goetz, K. P.; Vermeulen, D.; Payne, M. E.; Kloc, C.; McNeil, L. E.; Jurchescu, O. D., Charge-transfer complexes: new perspectives on an old class of compounds. *J. Mater. Chem. C* **2014,** *2*, 3065-3076.
15. Sutton, A. L.; Abrahams, B. F.; D'Alessandro, D. M.; Goerigk, L.; Hudson, T. A.; Robson, R.; Usov, P. M., Semi-conducting mixed-valent $X_4TCNQ^{I-/II-}$ (X = H, F) charge-transfer complexes with $C_6H_2(NH_2)_4$. *J. Mater. Chem. C* **2020,** *8*, 9422-9426.
16. Cohen, M. J.; Coleman, L. B.; Garito, A. F.; Heeger, A. J., Electrical conductivity of tetrathiofulvalinium tetracyanoquinodimethan (TTF) (TCNQ). *Phys. Rev. B* **1974,** *10*, 1298-1307.
17. Zhang, X.; Zhang, Z.; Zhao, H.; Mao, J.-G.; Dunbar, K. R., A cadmium TCNQ-based semiconductor with versatile binding modes and non-integer redox states. *Chem Commun.* **2014**, *50*, 1429-1431.
18. Heintz, R. A.; Zhao, H.; Ouyang, X.; Grandinetti, G.; Cowen, J., Dunbar K. R., New Insight into the Nature of Cu(TCNQ): Solution Routes to Two Distinct Polymorphs and Their Relationship to Crystalline Films That Display Bistable Switching Behavior. *Inorg. Chem.* **1999**, *38*, 144-156.
19. Ballesteros-Rivas, M.; Ota, A.; Reinheimer, E.; Prosvirin, A.; Valdés-Martinez, J.; Dunbar, K. R., Highly Conducting Coordination Polymers Based on Infinite M(4,4′-bpy) Chains Flanked by Regular Stacks of Non-Integer TCNQ Radicals. *Angew. Chemie - Int. Ed.* **2011**, *50*, 9703–9707.
20. Campana, C.; Dunbar, K. R.; Ouyang, X. A novel one-dimensional structure involving μ_4-TCNQ ligands and quadruply bonded dimolybdenum units (TCNQ = 7,7,8,8-tetracyanoquinodimethane), *Chem. Commun.* **1996**, 2427-2428.

21. Miyasaka, H.; Campos-Fernández, C. S.; Clérac, R.; Dunbar, K. R., Hexagonal Layered Materials Composed of $[M_2(O_2CCF_3)_4]$ (M = Ru and Rh) Donors and TCNQ Acceptors. *Angew. Chemie Int. Ed.* **2000**, *39*, 3831–3835.
22. Miyasaka, H.; Izawa, T.; Takahashi, N.; Yamashita, M.; Dunbar, K. R. Long-Range Ordered Magnet of a Charge-Transfer Ru_2^{4+}/TCNQ Two-Dimensional Network Compound. *J. Am. Chem. Soc.* **2006**, *128*, 11358–11359.
23. Motokawa, N.; Miyasaka, H.; Yamashita, M.; Dunbar, K. R. An Electron-Transfer Ferromagnet with T_c=107 K Based on a Three- Dimensional $[Ru_2]_2$/TCNQ System *Angew. Chemie Int. Ed.* **2008**, *47*, 7760–7763.
24. Miyasaka, H.; Motokawa, N.; Matsunaga, S.; Yamashita, M.; Sugimoto, K.; Mori, T.; Toyota, N.; Dunbar, K. R. Control of Charge Transfer in a Series of $Ru_2^{II,II}$/TCNQ Two-Dimensional Networks by Tuning the Electron Affinity of TCNQ Units: A Route to Synergistic Magnetic/Conducting Materials. *J. Am. Chem. Soc.* **2010**, *132*, 1532–1544.
25. Motokawa, N.; Matsunaga, S.; Takaishi, S.; Miyasaka, H.; Yamashita, M.; Dunbar, K. R. Reversible Magnetism between an Antiferromagnet and a Ferromagnet Related to Solvation/Desolvation in a Robust Layered $[Ru_2]_2$TCNQ Charge-Transfer System. *J. Am. Chem. Soc.* **2010**, *132*, 11943–11951.
26. Suchanski, M. R.; Van Duyne, R. P., Resonance Raman spectroelectrochemistry. IV. The oxygen decay chemistry of the tetracyanoquinodimethane dianion. *J. Amer. Chem. Soc.,* **1976,** *98*, 250-252.
27. Abrahams, B. F.; Elliott, R. W.; Hudson, T. A.; Robson, R.; Sutton, A. L., X_4TCNQ^{2-} dianions: versatile building blocks for supramolecular systems. *CrystEngComm* **2018,** *20*, 3131-3152.
28. Abrahams, B. F.; Elliott, R. W.; Hudson, T. A.; Robson, R.; Sutton, A. L., New $Cu^I_2(TCNQ^{-II})$ and $Cu^I_2(F_4TCNQ^{-II})$ Coordination Polymers. *Cryst. Gr. Des.* **2015,** *15*, 2437-2444.
29. Abrahams, B. F.; Elliott, R. W.; Robson, R., Coordination Polymers Constructed from $TCNQ^{2-}$ Anions and Chelating Ligands. *Aust. J. Chem.* **2014,** *67*, 1871-1877.
30. Saber, M. R.; Prosvirin, A. V.; Abrahams, B. F.; Elliott, R. W.; Robson, R.; Dunbar, K. R., Magnetic coupling between metal spins through the 7,7,8,8-tetracyanoquinodimethane (TCNQ) dianion. *Chem. Eur. J.* **2014,** *20*, 7593-7597.
31. Abrahams, B. F.; Elliott, R. W.; Hudson, T. A.; Robson, R., PtS-Related $\{[Cu^I(F_4TCNQ^{II-})]^-\}_\infty$ Networks. *Cryst. Gr. Des.* **2013,** *13*, 3018-3027.

32. Abrahams, B. F.; Elliott, R. W.; Hudson, T. A.; Robson, R., A new type of 3D $[M^{II}_2(TCNQ^{-II})_3]^{2-}$ coordination network with spacious channels of hexagonal cross-section generated from $TCNQH_2$. *CrystEngComm* **2012,** *14*, 351-354.
33. Abrahams, B. F.; Elliott, R. W.; Hudson, T. A.; Robson, R., A New Class of Easily Generated $TCNQ^{2-}$-Based Coordination Polymers. *Cryst. Gr. Des.* **2010,** *10*, 2860-2862.
34. Abrahams, B. F.; Hudson, T. A.; Robson, R., A New Approach to TCNQ-Based Coordination Polymers via $TCNQH_2$. *Cryst. Gr. Des.* **2008,** *8*, 1123-1125.
35. Shimomura, S.; Matsuda, R.; Tsujino, T.; Kawamura, T.; Kitagawa, S., TCNQ dianion-based coordination polymer whose open framework shows charge-transfer type guest inclusion. *J. Am. Chem. Soc.* **2006,** *128*, 16416-16417.
36. Shimomura, S.; Yanai, N.; Matsuda, R.; Kitagawa, S., Impact of metal-ion dependence on the porous and electronic properties of TCNQ-dianion-based porous coordination polymers. *Inorg Chem* **2011,** *50*, 172-7.
37. Kitaura, R.; Seki, K.; Akiyama, G.; Kitagawa, S., Porous coordination-polymer crystals with gated channels specific for supercritical gases. *Angew. Chem. Int. Ed. Engl.* **2003,** *42*, 428-431.
38. Tanaka, D.; Nakagawa, K.; Higuchi, M.; Horike, S.; Kubota, Y.; Kobayashi, T. C.; Takata, M.; Kitagawa, S., Kinetic gate-opening process in a flexible porous coordination polymer. *Angew. Chem. Int. Ed. Engl.,* **2008,** *47*, 3914-3918.
39. Abrahams, B. F.; Babarao, R.; Dharma, A. D.; Holmes, J. L.; Hudson T. A.; Maynard-Casely, H. E.; McGain, F.; Robson, R.; White, K. F., The Effect of Sterically Active Ligand Substituents on Gas Adsorption within a Family of 3D Zn-Based Coordination Polymers. *Inorg. Chem.*, **2020**, 59, 8871-8881.
40. Edubilli, S; Gumma, S. A systematic evaluation of UiO-66 metal organic framework for CO_2/N_2 separation. *Separation and Purification*, **2019**, 224, 85-94.
41. Cmarik, G. E.; Kim, M.;Cohen, S. M.; Walton, K. S.; Tuning the Adsorption Properties of UiO-66 via Ligand Functionalization, *Langmuir*, **2012**, 28, 15606-15613.
42. Spek, A. L., PLATON SQUEEZE: a tool for the calculation of the disordered solvent contribution to the calculated structure factors. *Acta Crystallogr. C Struct. Chem.* **2015,** *71*, 9-18.
43. Tauc, J., Optical properties and electronic structure of amorphous Ge and Si. *Mater. Res. Bull.* **1968,** *3*, 37-46.
44. Perdew, J. P.; Burke, K.; Ernzerhof, M., Generalized Gradient Approximation Made Simple. *Phys. Rev. Lett.* **1996,** *77*, 3865-3868.

45. Grimme, S.; Ehrlich, S.; Goerigk, L., Effect of the damping function in dispersion corrected density functional theory. *J. Comput. Chem.* **2011,** *32*, 1456-1465.

46. Yu, M.-H.; Space, B.; Franz, D.; Zhou, W.; He, C.; Li, L.; Krishna, R.; Chang, Z.; Li, W.; Hu, T.-L.; Bu, X.-H. Enhanced Gas Uptake in a Microporous Metal–Organic Framework *via* a Sorbate Induced-Fit Mechanism. *J. Am. Chem. Soc.* **2019**, *141,* 17703-17712.

47. Gao, Q.; Xu, J.; Cao, D.; Chang, Z.; Bu, X.-H. A Rigid Nested Metal-Organic Framework Featuring a Thermoresponsive Gating Effect Dominated by Counterions. *Angew. Chem. Int. Ed. Engl.,* **2016,** *55*, 15027-15030.

Table of Contents graphic